Acta Pharmacologica Sinica

www.nature.com/aps

ARTICLE

Combined in silico/in vitro approaches for identifying modulators of the activity of the p.Tyr110Cys Carnitine *O*-Acetyltransferase (CRAT) variant associated to an early onset case of Leigh syndrome

Lucas Cafferati Beltrame[1], Maria Noemi Sgobba[1], Luna Laera[1], Valeria Scaglione[1], Sabino Todisco[1], Serena Barile[1], Anna Lucia Francavilla[1], Danila Imperia De Luca[1], Michele Montaruli[1], Vito Porcelli[1], Lorenzo Guerra[1], Anna De Grassi[1]✉, Mariateresa Volpicella[1]✉ and Ciro Leonardo Pierri[2]✉

Carnitine *O*-acetyltransferase (CRAT) is a crucial enzyme involved in mitochondrial energy metabolism. Alterations in CRAT activity have emerged as significant contributors to the pathogenesis of Leigh syndrome and related mitochondrial disorders. In this study we employed an integrated approach combining in silico docking analysis and virtual screening of chemical libraries with subsequent in vitro validation to identify small molecule modulators of the activity of the wild type (WT) CRAT and the p.Tyr110Cys (Y110C) variant associated to an early onset case of Leigh syndrome. Through 3D molecular modeling, docking simulations, and virtual screening of chemical libraries, potential CRAT modulators were prioritized based on their predicted binding affinities and interactions with the 3D models of the WT-CRAT and of the p.Tyr110Cys-CRAT mutant. The performed in silico analyses were validated through in vitro assays on the purified recombinant CRAT proteins and cell-lysates from control fibroblasts and the fibroblasts of a patient with genetic diagnosis of CRAT-deficiency, carrying the compound heterozygous missense variants in the CRAT gene, namely p.Tyr110Cys and p.Val569Met. Based on the above screening by applying the indicated filtering strategy and mentioned criteria, 3 commercially available approved drugs (also known for their possible interactions with mitochondria) namely glimepiride, artemisinin and dorzolamide, as well as suramin (already known for its ability to interact with mitochondrial proteins) were tested in in vitro assays. We found that suramin (1−1000 µM) dose-dependently inhibited the activity of both WT-CRAT and p.Tyr110Cys_CRAT variant. Artemisinin (0.1–200 µM) dose-dependently stimulated the activity of the recombinant p.Tyr110Cys CRAT mutant, whereas glimepiride and dorzolamide did not change the activity of these proteins towards acetyl-CoA. This study demonstrates the effectiveness of this combined approach in identifying novel compounds for modulating CRAT enzyme activity, providing valuable insights for potential therapeutic interventions targeting CRAT-related disorders.

Keywords: carnitine acetyltransferase; Leigh-like syndrome; mitochondrial encephalomyopathy; 3D modeling and virtual screening of chemical libraries; suramin; artemisinin

Acta Pharmacologica Sinica (2024) 0:1–14; https://doi.org/10.1038/s41401-024-01435-0

INTRODUCTION

Leigh-like syndrome, characterized by progressive neurodegeneration, mitochondrial impairment, and metabolic dysfunction, represents a heterogeneous group of disorders with diverse genetic aetiologies [1–7]. Among the implicated factors, alterations in the activity of Carnitine O-Acetyltransferase (CRAT), a crucial enzyme involved in mitochondrial energy metabolism, have emerged as significant contributors to the pathogenesis of Leigh syndrome and related mitochondrial disorders [1].

CRAT catalyses the reversible transfer of acyl-groups (with different efficiency depending on the length and branching of the acyl chain) between carnitine and coenzyme A (CoA) and thus its activity is linked to acetyl-CoA/carnitine shuttle system on mitochondrial membrane. In this way, CRAT plays a pivotal role in the regulation of acyl-CoA/CoA ratio into mitochondrial matrix, which leverages on a plethora of pathways, including energy production through β-oxidation [1, 7].

Dysregulation of CRAT activity has been implicated in the disruption of mitochondrial function, leading to impaired energy production, oxidative stress, and ultimately cellular dysfunction [1, 7]. In particular, genetic mutations affecting CRAT have been identified in patients with Leigh-like syndrome, underscoring the importance of this enzyme in mitochondrial homeostasis and neurological function [1, 8].

---

[1]Department of Biosciences, Biotechnologies and Environment; University of Bari “Aldo Moro”, 70125 Bari, Italy and [2]Laboratory of Biochemistry, Structural and Molecular Biology, Department of Pharmacy – Pharmaceutical Sciences, University of Bari “Aldo Moro”, 70125 Bari, Italy
Correspondence: Anna De Grassi (anna.degrassi@uniba.it) or Mariateresa Volpicella (mariateresa.volpicella@uniba.it) or Ciro Leonardo Pierri (ciro.pierri@uniba.it)
These authors contributed equally: Lucas Cafferati Beltrame, Maria Noemi Sgobba, Luna Laera

Received: 31 August 2024 Accepted: 16 November 2024

The critical role of CRAT in mitochondrial metabolism, cell viability, and the pathogenesis of Leigh syndrome highlights the importance of identifying small molecule modulators of CRAT activity, as potential therapeutic interventions. Computational methods, based on structural comparative analyses, molecular docking and virtual screening of chemical libraries, have emerged as valuable tools for the identification and optimization of lead compounds targeting specific enzymes [2, 9–12]. These in silico approaches offer the advantage of screening a vast chemical space to prioritize potential candidates for further experimental validation [9, 10, 13].

In this study, we present an integrated approach that combines computational docking analysis and virtual screening with subsequent in vitro validation to identify novel modulators of CRAT enzyme activity. Leveraging three-dimensional (3D) modeling analyses of the wild-type (WT) CRAT and of the p.Tyr110Cys-CRAT proteins, we conducted virtual screening of chemical libraries to prioritize compounds with the potential to interact with key residues involved in CRAT activity. Furthermore, the accuracy of our computational predictions was rigorously validated through in vitro assays using recombinant CRAT proteins and cell lysates from a patient carrying the p.Tyr110Cys and the p.Val569Met variants, confirming the efficacy of identified compounds in modulating CRAT activity.

Through this integrated approach, we aim to contribute to the development of novel therapeutic strategies for the treatment of Leigh (and Leigh-like) syndrome and related mitochondrial disorders caused by CRAT impairment. At the same time, our study might represent a reference for investigating the activity of other enzymes with missense mutations causing a partial loss of function, involved in the onset of Leigh syndrome, aiming to identify selective modulators directed towards the investigated enzymes for stimulating/ameliorating their impaired activity.

MATERIALS AND METHODS

Strains and materials

XL-1 blue cells (Stratagene, San Diego, USA) were used as bacterial host, while Rosetta^{TM} 2(DE3) competent cells (Novagen®, Darmstadt, Germany) were used for the expression of the recombinant proteins. Unless specifically indicated, all DNA manipulations were performed according to standard procedures. The wild-type CRAT mRNA sequence (NM_000755.4) and a 5′ 6×His-tag were assembled into a pET-21a(+) plasmid purchased from Genscript® (New Jersey, USA) (OHu15347). The p.Tyr110Cys recombinant pET-21a(+) plasmid was obtained as previously described [1] and was checked by Sanger sequencing using the Eurofins Genomic Support (Luxembourg, Luxembourg).

Acetyl-CoA (A2056), *L*-carnitine (C0158), dorzolamide (SML0468), glimepiride (G2295) and suramin (S2671) were purchased from Sigma (Saint Louis, USA); artemisinin (sc-202960) was purchased from Santa Cruz Biotechnology (Dallas, USA).

Expression and purification of recombinant CRAT proteins

The expression of the recombinant WT-CRAT and p.Tyr110Cys CRAT variant was obtained after 5 h induction with isopropyl β-*D*-1-thiogalactopyranoside (IPTG) at a final concentration of 1 mM, following the protocol reported in [1]. Expressed bacterial cells were then collected by centrifugation at 6000 rpm for 10 min at 4 °C, diluted in buffer solution (0.5 M NaCl, 10 mM PIPES pH 7.0) containing 10 mM imidazole and lysed with French press. After centrifugation at 14,000 rpm for 20 min at 4 °C, the supernatant was incubated with a nickel-charged resin (Ni-NTA Agarose, QIAGEN, Hilden, Germany) under shaking. The nickel-charged resin was washed using buffers at increasing concentrations of imidazole to remove nonspecific-bounded proteins, and CRAT proteins were finally eluted using a 100 mM imidazole buffer solution. The purity of recombinant CRAT proteins was assessed by 12% SDS-PAGE. All the purified recombinant proteins were concentrated using the Amicon® Ultra 0.5 mL Centrifugal Filters 30 K (Merck Millipore, Burlington, USA) and then resuspended in storage buffer (25 mM Tris/HCl pH 7.3, 1 mM EDTA, 100 mM glycine, 10% glycerol, 0,05% sodium azide). The concentration of the purified recombinant proteins was determined using the standard curve produced with BSA at triplicate points of 1, 2, 3, 4, and 5 µg.

Activity assays on the recombinant CRAT in the presence of the investigated molecules

CRAT specific activity was measured by a spectrophotometric assay using the Varian Cary® 50 UV-Vis Spectrophotometer (Agilent, Santa Clara, USA), as already reported in [1]. The different molecules were solubilized as 10× stocks as reported: i) suramin at 10 mM in ultrapure water; ii) a stock of 155 mM of dorzolamide in DMSO was diluted to 10 mM in ultrapure water; iii) glimepiride at 10 mM in DMSO, and iv) artemisinin at 100 mM in DMSO, following diluted at 1 mM in ultrapure water. All reactions were carried out in a final volume of 1 mL. Baseline measurements of absorbance were performed by incubating for 1 min the first sample aliquot (containing 300 ng of protein) in a reaction buffer (50 mM Tris-HCl pH 8.00, 1 mM EDTA pH 8.00, 0.1 mM DTNB, 0.1 mM acetyl-CoA). Then the reaction was started by adding carnitine (at the final concentration of 2 mM in the cuvette) and the enzyme activity was then monitored in the absence (Control) or in the presence of the investigated molecules by measuring the rate of reduction of DTNB to TNB (412 nm) for a further 4 min. The absorbance variation in the linear range (about 2 min) was used for the specific activity calculation. All control tests (without molecules) were performed in water (i.e. used as a control for suramin that was solubilized in water) or in the presence of the same DMSO concentration used in the assays performed in the presence of the molecules solubilized in DMSO (i.e. artemisinin, glimepiride, dorzolamide). All the assays were performed at least in triplicate.

Determination of CRAT enzymatic activities in cultured fibroblasts

Primary dermal fibroblasts were cultured at 37 °C, 5% CO_2 in DMEM High gluclose (Elabscience Houston, USA, PM150210A), with 20% FBS (Euroclone, Pero, Italy, ECS0180L) and 1% penicillin-streptomycin (Euroclone, ECM0010D). 90% confluent cells were harvested with 0.25% trypsin treatment (Elabscience, PB180225) and counted (Luna II Automated Cell Counter).

Citrate synthase activity was assessed using a spectrophotometric assay [14]. Subsequently the same protocol was adapted for measuring carnitine acetyltransferase activity [1]. Briefly, 2×10^6 control fibroblasts and 2×10^6 patient fibroblasts (carrying the compound heterozygous missense variants in the CRAT gene, namely p.Tyr110Cys and p.Val569Met [1]) were lysed with a cell lysis buffer (150 mM KCl, 25 mM Tris-HCl pH 8.00, 2 mM EDTA pH 8.00, 10 mM KH_2PO_4, 0.1% BSA and 30 µM digitonin) and the protein concentration quantification was performed by DC protein assay purchased from BIO-RAD (Hercules, USA). The obtained samples from control fibroblasts and from patient fibroblasts were divided in two series of aliquots. Baseline measurements of absorbance (Varian spectrophotometer, Cary 50 UV-Vis) were obtained by incubating the first sample aliquot, namely 30 µg of proteins from control fibroblasts or from patient fibroblasts (1 min), in a reaction buffer (50 mM Tris-HCl pH 8.00, 1 mM EDTA pH 8.00, 0.1 mM DTNB, 0.45 mM acetyl-CoA). Citrate synthase activity was determined by measuring the rate of reduction of DTNB to TNB (412 nm) by the free CoA-SH liberated from acetyl-CoA after adding 2 mM oxaloacetic acid and monitoring for 5 min. Carnitine acetyltransferase was determined on the second sample aliquot (30 µg of proteins from control fibroblasts and patient fibroblasts) using the same protocol and replacing 2 mM oxaloacetic acid by 2 mM *L*-carnitine. All the assays were performed on cell-lysates in the presence and absence of the artemisinin solubilized in DMSO at two different concentrations

(0.01 and 0.1 mM) in the reaction volume (1 mL). For each assay, 10 µL of the prepared artemisinin solutions at the indicated concentrations, or 10 µL of DMSO, or 10 µL of ultrapure water, as control, wasemployed in the analysis. The final reaction volume contained 1% DMSO (*v*/*v*) in assays involving artemisinin and in corresponding assays with DMSO alone. The absorbance variation in 2 min was used as a relative estimate of enzymatic activity.

Statistical analysis

All in vitro experiments were conducted in three independent replicates. Data are presented as mean ± SEM for the enzymatic activity determination. K_m and V_{max} values are shown with 95% confidence intervals and asterisks (***) denote non-overlapping 95% confidence intervals between WT protein and the p.Tyr110Cys variant, as previously described [1]. For the dose-response experiments, IC_{50} values for suramin and EC_{50} values for artemisinin were calculated according to well established protocols [10, 15]. Comparative analyses were performed using the *t*-test, with statistical significance defined as $P\text{-value} < 0.05$ ($*P < 0.05$; $**P < 0.01$; $***P < 0.001$). All statistical analyses were performed using GraphPad Prism v.8.0.1.

3D comparative modeling of CRAT p.Tyr110Cys mutant protein

The PyMOL software was used to visualize the high-resolution crystallized structure of the wild-type human CRAT protein (1nm8.pdb, resolution 1.8 Å [16]). The binding poses and atomic coordinates of CRAT substrates, i.e. carnitine, CoA, acetyl-CoA, within the studied CRAT protein structure (1nm8.pdb, [16]) were obtained as previously described [1]. More in detail, the structure of the available Crat proteins crystallized in complex with carnitine, CoA and acetyl-CoA (the murine 2h3p.pdb, resolution 2.2 Å [17]), or with carnitine and CoA (the murine 2h3u.pdb), were superimposed to the human CRAT (1nm8.pdb) and the coordinates of the substrates taken from the cited crystallized structures superimposed to 1nm8.pdb were duplicated and saved in a new ".pdb" file together with the human CRAT (from 1nm8.pdb). Acetylation of carnitine was obtained in silico by using the build tool implemented in PyMOL, as previously reported [1].

The 3D model of the CRAT p.Tyr110Cys mutant protein was generated by using the in silico mutagenesis analysis tool implemented in PyMOL according to protocols previously described [1, 9].

Three cycles of 100 steps of steepest descent energy minimization were performed on the WT protein refined from 1nm8.pdb structure, as well as on the generated p.Tyr110Cys 3D mutant model, by using the energy minimization tool implemented in SwissPDBViewer (SPDBV), and the correct 3D model packing was verified also by manual inspection by PyMOL.

Docking analysis

To find highly selective ligands for the investigated CRAT binding region we performed a virtual screening of an in-house developed chemical library by using AutoDock 4 [10, 18, 19]. The chemical library used for the Virtual Screening contains 10977 ligands including: drugs, natural and synthetic compounds, toxins, metabolism products and biologically active substances. The main sources for these molecules are the freely available KEGG_DRUG and KEGG_COMPOUNDS [10, 20] databases (all the selected molecules show a molecular weight between 5 and 2100 Dalton). The molecules of the library have been optimized with openBabel [21] by generating energy-minimized 3D conformers before being used in the virtual screening. The charges associated with molecules in the library were determined by openBabel based on their protonation states at pH 7.8 (typically observed in the matrix of mammalia mitochondria [22–24]) before performing docking analysis.

Before proceeding with the virtual screening, the CRAT wild-type protein and the CRAT p.Tyr110Cys mutant were prepared for the docking simulation converting both protein ".pdb" files in a ".pdbqt" file by using the MGLTools of Autodock [10, 19]. The ".pdbqt" file contained gasteiger charges for every atom present in the original and mutant CRAT ".pdb" files. Similarly, all the ligands (".mol2" files) contained in our chemical library (energetically minimized) were converted in ".pdbqt" files for the virtual screening by using the Autodock scripts [10, 19].

In order to validate our docking protocols, firstly we performed a set of re-docking simulations [9, 10] by using Autodock 4.2, on the WT protein deprived of carnitine, by varying gridbox size and center, aiming to reproduce the same carnitine poses obtained in the reference structure consisting of the superimposed CRAT atomic coordinates, taken from 1nm8.pdb, and carnitine/CoA atomic coordinates, taken from the 2h3u.pdb protein complex.

For each re-docking simulation the parameter "rmstol" was set to 1.5 Å; the parameter "ga_pop_size" was set to 150, the parameter "ga_num_evals" was set to 2.5×10^5, the parameter "ga_num_generations" was set to 2.7×10^4. The number of top individuals to survive to the next generation was set to 5 and a ranked cluster analysis of the 50 ligand poses generated was performed. For details about the significance of the above reported parameter names see Morris et al. [25].

The gridbox that better reproduced the pose of the wild-type CRAT in complex with carnitine (according to the procedure above described) consists of 52 × 58 × 62 gridpoints in the x–y–z Cartesian space centered on the point of coordinates 44.16 (x), 27.909 (y), 9.805 (z). The spacing, namely the distance between adjacent gridpoints within the gridbox, was set to 0.286 Å. Obtaining a good re-docked conformation (i.e., a pose of the carnitine-ligand within the carnitine substrate binding region very similar to the carnitine pose observed in the crystallized complex) allows establishing residues most likely directly involved in interactions with carnitine. The re-docked conformation and the reference carnitine ligand have been used as a reference system, e.g. to classify all the screened ligands as probable higher affinity or lower affinity small molecules, by using as discriminant and positive control, the relative binding energy calculated for the best re-docked CRAT-carnitine protein-ligand complex conformation.

Before proceeding with the virtual screening, a single docking analysis of carnitine in the CRAT p.Tyr110Cys mutant model (in the absence of carnitine) was also performed by using the same gridbox employed in the above-cited re-docking analysis.

Being the mutation p.Tyr110Cys the only difference between the investigated mutant and the wild-type protein, we used the same gridbox consisting of 52 × 58 × 62 gridpoints in the x–y–z Cartesian space centered on the point of coordinates 44.16 (x), 27.909 (y), 9.805 (z) for screening our ligand library with the goal to find a small molecule that can mimic the aromatic portion of the native tyrosine 110 residue observed in the WT protein. The carnitine ligand was maintained during the docking-based virtual screening in the native position observed in the above cited WT-CRAT-carnitine complex structure, aiming to find a molecule able to bind close to the mutation position C110, for mimicking the Y110 natively present in the WT.

In our docking-based virtual screening we chose to use the Lamarckian Genetic Algorithm [10, 26]. For each ligand of our library 20 runs were performed; the parameter "rmstol" was set to 0.5; the parameter "ga_pop_size" was set to 150 and the parameter "ga_pop_evaluations" was set to 1×10^6. At the end of the simulation, we built a list sorted by energy of the lowest energy docking for each ligand for a total of 10,008 successfully screened ligands (the complete list is available upon request).

Among the remaining 969 ligands, 245 ligands produced positive binding values most likely due to their great size. 33 out of the 245 ligands are approved drugs and for this group of drugs, it was chosen to perform a second screening by using a dedicated gridbox with the same gridcenter of the one used in the re-docking simulation but with more gridpoints (88, 88, 88 gridpoints along the x, y, z axis, respectively). Carnitine ligand was mantained in the carnitine binding pocket also in this second small screening of the 33 drugs.

From the docked ligands, four molecules were chosen for other dedicated analysis. More in detail, a single docking analysis with the four selected molecules was performed, in the gridboxes prepared as above described, either on the wild-type CRAT or on the CRAT p.Tyr110Cys mutant protein, in the presence and absence of the carnitine substrate.

Choice of molecules predicted with high affinity for the in vitro assays

It was chosen to test in vitro a restricted set of molecules with a predicted negative binding energy for the carnitine binding region within the CRAT protein, based on the below reported criteria:

1. the existence of known pharmacological properties of the selected molecule;
2. known relationships between the selected molecules and mitochondria;
3. known relationships between the selected molecules and carnitine or proteins able to interact with carnitine;
4. their solubility and compatibility with the experimental setup;
5. number of atoms/torsions in relation to the gridbox size;
6. the ability of the molecules to bind a region close to the p.Tyr110Cys mutation, ideally conferring the ability to re-orient carnitine ligand towards its correct binding pose in the p.Tyr110Cys CRAT mutant protein.

RESULTS

3D molecular modeling of p.Tyr110Cys CRAT mutant and re-docking analysis

To build the p.Tyr110Cys CRAT mutant protein we used the mutagenesis tool implemented in PyMOL to replace the Y110 residue with a cysteine residue. The replacement of Y110 with a cysteine residue caused a local re-arrangement of the helix at the level of the investigated mutation and an increase in the distance from the substrate, even more visible after the energy minimization (Fig. 1).

It is observed that residues within 4 Å either from the crystallized or from the docked carnitine in the wild-type protein are the same. Among them, H343, E347, Y452, S454, T465, S552, T553, V569 and F566 form a pocket with aromatic/hydrophilic features surrounding carnitine ligand (Fig. 1c).

Conversely, the docking of carnitine in the p.Tyr110Cys mutant produces a re-oriented pose of carnitine in the explored binding region including a set of interactions with different residues such as A106, Y107, I116, Y117, P120, and with residues H343, F566 already bound by carnitine in the WT protein (Fig. 1d).

Re-docking on the wild-type protein

The re-docking simulation allowed us to define a specific gridbox for the human CRAT that was able to reproduce the crystallized protein–substrate complex with high fidelity. The root mean square deviation (RMSD) between the coordinates of the ligand in the crystallized complex and the best “re-docked” pose coordinates, obtained by using Autodock, was equal to 1.1 Å Fig. 1c. The resulting binding energy calculated by Autodock was equal to −3.55 kcal/mol. The same gridbox was used for docking carnitine in the p.Tyr110Cys CRAT mutant, providing the docked-pose

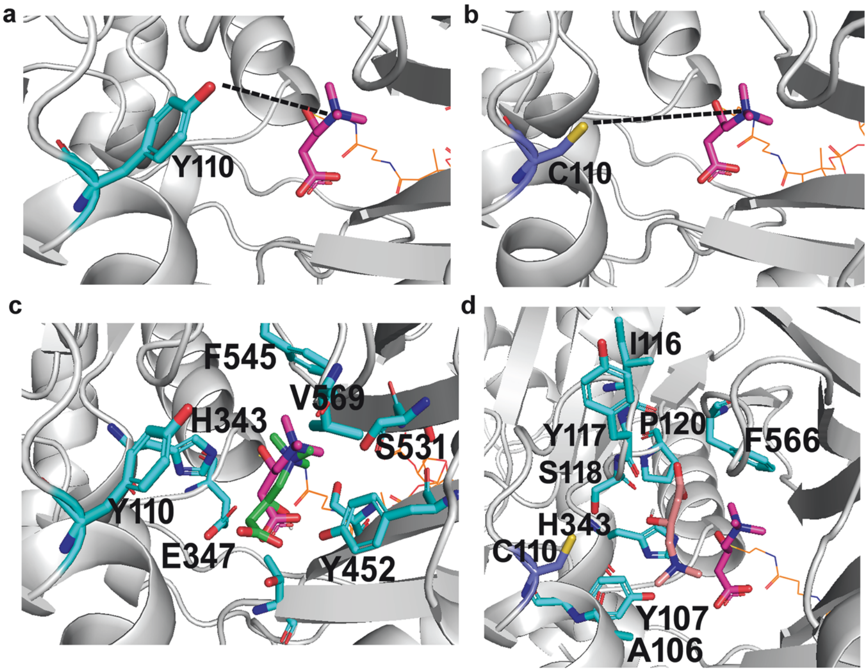

Fig. 1 3D structure of the CRAT wild-type protein and of the p.Tyr110Cys investigated 3D mutant. a WT-CRAT protein 3D crystallized structure is reported in white cartoon representation. Y110 is reported in white sticks. The dashed line indicates the distance of 8.3 Å between Y110 and carnitine. **b** The p.Tyr110Cys CRAT mutant is reported in white cartoon representation and C110 is reported in pink sticks. Carnitine and CoA are reported in both panels in magenta sticks and orange lines, respectively. The dashed line indicates the distance of 10.6 Å between C110 and carnitine. **c** Re-docking of the carnitine ligand in the wild-type CRAT. The RMSD between atomic coordinates of the reference carnitine structure (magenta) and the docked carnitine ligand (green) was 0.9 Å. Tyrosine 110 is reported in cyan sticks. **d** Docking of the carnitine ligand in the p.Tyr110Cys CRAT mutant protein. The generated docked poses of carnitine did not overlap at all with the reference carnitine structure (magenta sticks). The carnitine pose docked within p.Tyr110Cys mutant CRAT with the highest binding energy is reported in salmon. CoA is reported in orange lines also in panels **c** and **d**. Residues within 4 Å from the docked carnitine in the wild-type and mutant proteins are reported in cyan sticks. Both docking analyses were performed by using the first gridbox described in the methods.

observable in Fig. 1d, which showed no superimposition with the carnitine ligand observed in the crystallized structure and appeared much closer to the cysteine residue. The resulting binding energy calculated by Autodock was equal to −3.78 kcal/mol.

Virtual screening on the p.Tyr110Cys mutant in the presence of carnitine ligand whose coordinates were taken from the crystallized pose

Given that the investigated mutant showed only the replacement of Y110 with a cysteine, we decided to use the same gridbox for performing a docking-based virtual screening of our chemical library on the human p.Tyr110Cys CRAT mutant 3D model. The list sorted by energy of the 10,008 out of 10,977 successfully screened ligands showed a free energy of binding between −18.6 and −0.03 kcal/mol, number of atoms between 2 and 67, number of torsions between 0 and 31.

The first 399 molecules, showing a free energy of binding between −18.6 and −10.01 kcal/mol (number of atoms between 23 and 59; number of torsions between 0 and 25), were excluded from the following analyses because we considered very high the likelihood to find strong inhibitors among those molecules that appear very good binders, whereas we were more interested in finding an activator of the CRAT mutant.

We also excluded the last 1774 molecules showing a free energy of binding between −5.00 and −0.03 kcal/mol (number of atoms between 2 and 67; number of torsions between 0 and 31) for the high likelihood to identify ineffective ligands (among those molecules) given that the free energy of binding of those ligands was close to the free energy of binding estimated for carnitine (−3.78 kcal/mol).

Then, we searched along the list of the remained 7835 screened docked ligands for small molecules already approved as drugs and we recognized 1212 small molecules (drugs) still showing a free energy of binding between −10.00 and −5.01 kcal/mol.

From those molecules we excluded by visual inspection and literature search those that might present solubility problems (i.e., molecules whose solubility in water/DMSO was not described) and/or compatibility problems with the experimental set-up (i.e. ligands with free thiol groups, which may interact with DTNB/CoA, or colored ligands that can interfere with our absorbance reads at 412 nm were automatically excluded). As an example, cardiogreen, reactive-blue, beta carotene, and brucine were excluded at this level from the following analyses for their abilities in creating interferences with our spectrophotometric assay (with reads at 412 nm).

In addition, we searched on ChEMBL [27] for described interactions between the investigated molecules and mitochondria and/or carnitine and/or enzymes able to interact with carnitine and we excluded those molecules that did not show those interactions. In example, meticrane, argatroban, ramatroban, tetranactin, pazufloxacin, benzthiazide, and rottlerin were excluded at this stage from the following analyses because no piece of evidence about their possible interactions with mitochondria and/or carnitine metabolism has been proposed, yet.

Notably, 969 out of the 10,977 tested ligands showed a positive binding energy, between +0.01 and 987,000 kcal/mol (number of atoms between 23 and 105; number of torsions between 0 and 32). Given that some molecules (out of the 10,008) hosting 59 or 67 atoms have been successfully docked, providing negative binding energies along docking simulations, it was considered that the tested gridbox was too small for allowing molecules with a number of atoms between 68 and 105 (245 molecules, among which 33 approved drugs) to correctly explore it, to establish stabilizing interactions with residues of the investigated pocket. For verifying if the gridbox size was the real problem, a dedicated gridbox with the same gridcenter but more gridpoints (88, 88, 88) was tested on the 33 approved drugs (out of the 245 molecules cited above). The list sorted by energy of the 28 out of the 33 drugs successfully screened showed a free energy of binding between −16.89 and −4.17 kcal/mol, number of atoms between 69 and 98, number of torsions between 9 and 31. The complete list of the screened molecules in the two virtual screenings is available upon request. At the end of the above screening, by applying the indicated filtering strategy and mentioned criteria, we decided to test in in vitro assays 3 commercially available approved drugs (also known for their possible interactions with mitochondria) chosen from the first larger screening, namely glimepiride, artemisinin, and dorzolamide. In addition, 1 more molecule was chosen from the small screening of the above cited 33 drugs, namely suramin (already known for its ability to interact with mitochondrial proteins), to be tested in in vitro assays. The selected four molecules showed negative binding energies, being the first three in the −5.5 / −9.26 binding energy range, whereas suramin showed −11 kcal/mol (Fig. 2).

The docking analysis of the first three molecules provided strong indications for the possible binding of a protein region located between the region hosting C110 and the carnitine pose observed in the wild-type crystallized protein (see Fig. 3), whereas suramin appeared to behave as a plug fulfilling all the explored binding cavity.

The four selected molecules were thus re-docked on the wild-type CRAT (in the absence and presence of carnitine) to verify how the orientation of the investigated molecules changed in the presence of the native Y110 within the investigated binding pocket, either in the presence or in the absence of the carnitine ligand. It was observed that the presence of Y110 pushes the ligands closer to the region normally occupied by carnitine, if the carnitine is not maintained in the docking analysis. I.e., artemisinin and dorzolamide in the absence of carnitine almost overlaps carnitine (reported in lines representation for comparative purposes, Fig. 4b, e, respectively) compared to what happens in the presence of carnitine (reported in sticks representation, Fig. 4a, d). In addition, the presence of carnitine causes a re-orientation of dorzolamide and glimepiride to the bottom portion of the investigated pocket, as can be observed from the formation of new interactions between dorzolamide/glimepiride and T465 (Fig. 4e, h). Conversely, artemisinin appears to locate closer to the upper region of the investigated pocket (as demonstrated by the presence of I116 within 4 Å from artemisinin, Fig. 4b).

The larger suramin continues to occupy a similarly located region at the entry of the investigated pocket hosting carnitine in the crystallized structure forming interactions with the more external T105, L521, M547, F549 residues, both in the WT-CRAT and the CRAT-p.Tyr110Cys mutant, either in the presence or absence of carnitine, although in the absence of carnitine it appears to penetrate at a deeper level the investigated binding pockets (Fig. 4j–l).

Expression of the recombinant WT-CRAT and p.Tyr110Cys CRAT mutant proteins

The recombinant proteins, WT-CRAT and p.Tyr110Cys CRAT mutant, were expressed in *Escherichia coli* Rosetta 2(DE3) and then purified using affinity chromatography as reported in Materials and Methods (Fig. 5). The apparent molecular weight of the purified proteins was around 65 kDa, in good agreement with its theoretical molecular mass (calculated value starting from methionine, 70.7 kDa) (Fig. 5, lanes 3 and 6). As shown in Fig. 5 (lanes 1/2 and lanes 4/5), the two recombinant proteins were not detected in bacteria harvested immediately before the induction with IPTG. The yield of the purified proteins, quantified by SDS-PAGE analysis (see Fig. 5) was around 2.48 g for WT-CRAT and 3.35 g for the p.Tyr110Cys CRAT mutant, per liter of culture.

Activity assays of the recombinant WT-CRAT and p.Tyr110Cys proteins

The enzyme activity of the recombinant 6xHis-tagged WT-CRAT and p.Tyr110Cys CRAT mutant, expressed in *Escherichia coli* and purified

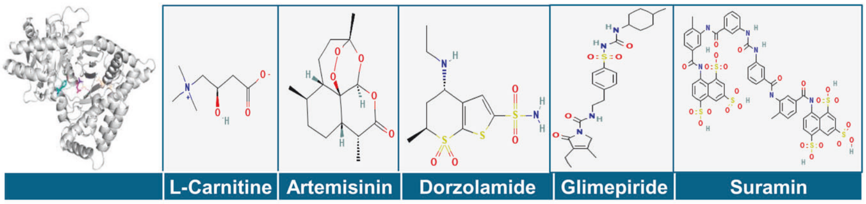

	L-Carnitine	**Artemisinin**	**Dorzolamide**	**Glimepiride**	**Suramin**
KeggDrug	D02176	D02481	D00653	D00593	D00808
KeggCompound	C00318	C09538	C06969	C07669	C07974
CID	10917	68827	5284549	3476	5361
MW (g/mol)	161.20	282.33	324.4	490.6	1297.3
WT CRAT + Carnitine LE/LC	**-3.55**	-7.87	-8.33	-10.7	-11.6
WT CRAT – Carnitine LE/LC	NA	-7.95	-8.75	-11.64	-9.14
CRAT Y110C + Carnitine LE/LC	**-3.78**	-6.85	-8.77	-9.26	-11.94
CRAT Y110C – Carnitine LE/LC	NA	-8.01	-8.37	-9.07	-8.19
N. atoms	12	20	23	36	92
N. torsions	5	0	4	7	16

Fig. 2 Free energy of binding (LE_LC, expressed in kcal/mol) calculated by autodock for the selected 4 molecules. The LE_LC (namely the energy of the Lowest Energy conformation in the Largest Cluster identified along autodock runs) for the re-docking of carnitine in the WT-CRAT or in the p.Tyr110Cys variant is reported in green characters or red characters, respectively, for comparative purposes. All the other free energy of binding of the investigated molecules for the WT-CRAT or for the CRAT-p.Tyr110Cys mutant were calculated either in the presence or in the absence of the carnitine ligand. 2D structures of the assayed ligands are also reported.

using affinity chromatography, was tested at several concentrations (1–100 μM) of acetyl-CoA, namely the main CRAT-specific substrate in mitochondria. The estimated Michaelis–Menten constant (K_m) and maximum activity rate (V_{max}) of acetyl-CoA for WT-CRAT were 20.39 μM, and 172.2 $\mu mol \cdot min^{-1} \cdot mg^{-1}$ protein, respectively, whereas the corresponding parameters for the p.Tyr110Cys variant were 14.92 μM, and 107.1 $\mu mol \cdot min^{-1} \cdot mg^{-1}$ protein. Each recombinant enzyme's activities adhered to the classical Michaelis–Menten kinetics model (Fig. 6a), enabling the determination of the V_{max} and the K_m of WT-CRAT and p.Tyr110Cys_CRAT proteins for acetyl-CoA. The CRAT p.Tyr110Cys variant predominantly affected interactions with acetyl-CoA, resulting in a reduction of both K_m for acetyl-CoA (Fig. 6b) and V_{max} (a loss of 38% in V_{max} compared to wild-type V_{max}, Fig. 6c).

In addition, in order to estimate the ability of the screened compounds in stimulating the activity of the investigated WT-CRAT and p.Tyr110Cys CRAT mutant, a saturating concentration of the substrate acetyl-CoA (100 μM), was incubated with the protein in the presence (M) and absence (C) of the screened selected compounds (dorzolamide, glimepiride, suramin and artemisinin) (Fig. 6d). To start the reaction, 2 mM carnitine was added and the reduction of DTNB was monitored as described in the methods section in the presence (M) and absence (C) of the selected molecules at the concentration of 1 mM except for artemisinin that was incubated at 100 μM, since 1 mM artemisinin started to precipitate in the tested conditions. Due to the fact that artemisinin, dorzolamide and glimepiride need to be solubilized in a DMSO/H_2O mix, each control for the three molecules was performed considering the DMSO:H_2O ratio used to solubilize and dilute each molecule (see the methods section) and assays were performed in the presence (M, for testing molecules) or in the absence (C, as a control) of the indicated molecules (Fig. 6d). The final DMSO/H_2O ratio in the cuvette was 0.1% for artemisinin, 0.64% for dorzolamide, 10% for glimepiride. Notably, suramin was soluble in water and the control test of suramin contained only water and this control has been used also as a general control (100% of CRAT activity, Fig. 6d). It is observed that the DMSO employed at the indicated final % did not affect significantly the activity of the investigated WT-CRAT and p.Tyr110Cys CRAT variant (Fig. 6d).

Glimepiride and dorzolamide did not result in significant activity variations of the investigated proteins towards acetyl-CoA, whereas suramin appears to severely inhibit the activity of both WT-CRAT and p.Tyr110Cys CRAT variant (Fig. 6d). Conversely, artemisinin appears to weakly stimulate the activity of p.Tyr110Cys CRAT mutant (Fig. 6d).

To investigate in a more detailed way the effect of suramin and artemisinin on the recombinant WT-CRAT and p.Tyr110-Cys_CRAT variant proteins, a dose-response analysis was performed in the presence of increasing concentrations of the two molecules (range 1 μM – 1 mM for suramin, 0.1–200 μM for artemisinin). It was observed that the WT-CRAT inhibition by suramin was between 20% (at concentrations lower than 10 μM) and >60% (at concentrations higher than 100 μM) with an $IC_{50} = 48$ μM on the WT-CRAT protein. Regarding p.Tyr110Cys, suramin inhibition was between 50% (at concentrations lower than 10 μM) and >80% (at concentrations higher than 100 μM) with an $IC_{50} = 49$ μM (Fig. 6e). Conversely, the stimulation of the activity of the p.Tyr110Cys CRAT mutant by artemisinin was between 11% (at concentrations lower than 10 μM) and 22% (at concentrations greater than 10 μM) with an $EC_{50} = 0.4$ μM. No evident stimulation effect mediated by artemisinin was observed on the WT-CRAT (Fig. 6f).

In vitro assays on cell-lysates from control and patient fibroblasts
To further investigate the effect of artemisinin on CRAT activity, the molecules were administered at two concentrations (0.01 mM and 0.1 mM) to cell-lysates obtained from control fibroblasts or from fibroblasts derived from a patient carrying the compound heterozygous missense variants p.Tyr110Cys and p.Val569Met in the CRAT gene. CRAT activity was normalized for citrate synthase (CS) activity estimated in parallel in the same conditions. Considering that the normalized CRAT activity from patient cells was 30% of CRAT activity observed in control fibroblasts, the administration of artemisinin to cell lysates prepared from patient fibroblasts increased the normalized CRAT activity already at 10 μM and at a greater extent at 100 μM, whereas a lower stimulation of CRAT activity was observed on cell-lysates from control fibroblasts hosting the WT-CRAT (Fig. 7).

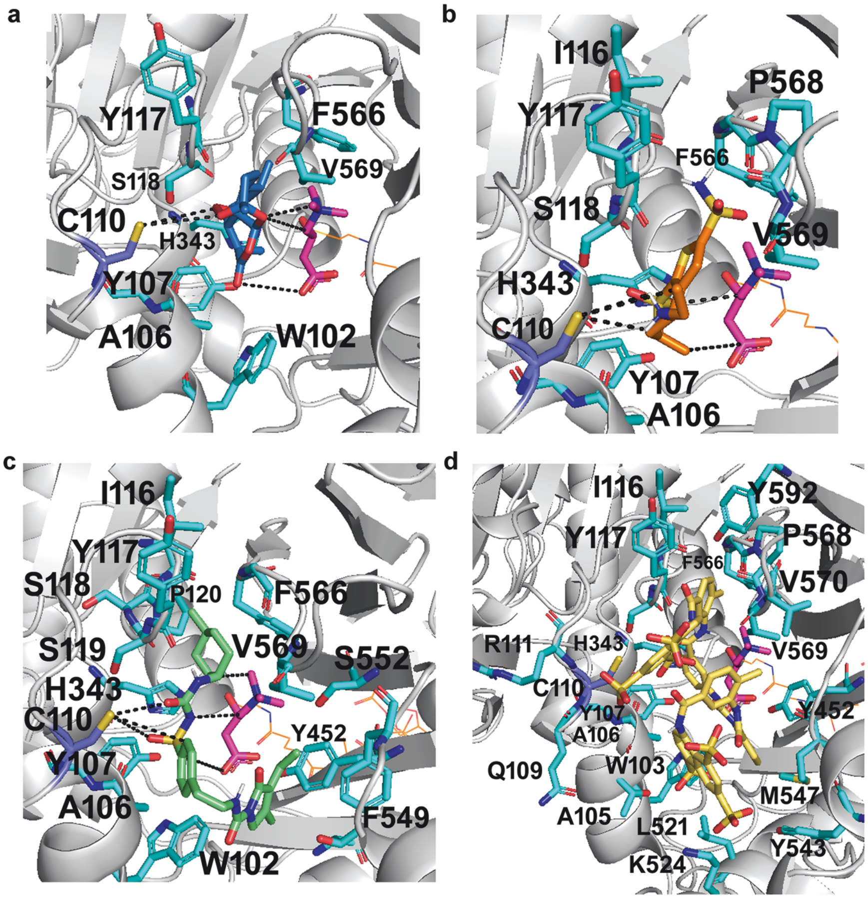

Fig. 3 Best poses of ligands artemisinin, dorzolamide, glimepiride, and suramin docked in the p.Tyr110Cys CRAT mutant. The best pose of artemisinin (**a**, blue sticks), dorzolamide (**b**, orange sticks), glimepiride (**c**, light green sticks), and suramin (**d**, light yellow sticks) docked in the p.Tyr110Cys CRAT mutant. C110 is reported in violet/yellow sticks, carnitine from the crystallized structure is reported in magenta sticks, CoA from the crystallized structure is reported in orange lines, whereas the p.Tyr110Cys CRAT protein is reported in white cartoon representation. Residues within 4 Å from the docked ligands are reported in cyan sticks. The best poses of Artemisinin, Dorzolamide, and Glimepiride were obtained by exploring the first described gridbox, whereas the reported best pose of Suramin was obtained by exploring the second larger described gridbox. Dashed lines were used for indicating some H-bond interactions below 4 Å for the first three molecules in panels **a**–**c**. In the case of suramin, those interactions were not highlighted for making less complicate the reading of residues labels.

DISCUSSION

Although the oxidative phosphorylation is an ancient pathway, selected along the evolution for generating ATP [28–30], present in most living organism hosting mitochondria, it is involved in a large network of pathways that can be seriously damaged by mutations affecting either respiratory chain complexes, or ATP synthase subunits, but also other proteins located within the intermembrane space, or embedded in the inner mitochondrial membrane, or located within the mitochondrial matrix, as also observed for the investigated CRAT variants recently associated to an early onset case of Leigh syndrome [1–3, 31, 32].

The case of CRAT variants

Between the two compound heterozygous missense variants p.Tyr110Cys and p.Val569Met, seriously impairing CRAT function and associated to an early onset case of Leigh syndrome [1], we chose to investigate the p.Tyr110Cys mutation, more dramatic from a structural point of view, attempting to rescue the p.Tyr110Cys CRAT variant function.

The replacement of Y110 with a cysteine residue in the CRAT protein resulted in a local rearrangement of the helix at the mutation site [1], as expected for the replacement of a tyrosine residue (more hydrophobic and performant in the stabilization of alpha helices) with a cysteine residue (more hydrophilic and performant in the stabilization of beta-sheets) [33, 34].

Our molecular modeling and docking analyses based on well-established protocols [9, 10] further revealed distinct orientations of the carnitine ligand within the binding pocket of the p.Tyr110Cys mutant compared to the wild-type protein, indicating alterations in substrate binding due to the mutation (the RMSD between the two docked poses was higher than 4 Å).

Docking-based screening for predicting CRAT high-affinity ligands

Central to our investigation was the strategy of identifying small molecule modulators capable of influencing CRAT activity. Leveraging computational modeling and virtual screening techniques [9, 10], we targeted the region surrounding the p.Tyr110Cys mutation, strategically located near the carnitine binding catalytic site [1]. By exploring this region in both wild-type and mutant CRAT proteins, and in the presence or absence of the substrate in the catalytic pocket, we aimed to identify compounds, which continued to bind the p.Tyr110Cys mutant at the same level (between the p.Tyr110Cys mutation and the carnitine pose observed in the crystallized WT-CRAT), independently on the presence of the carnitine ligand in docking analysis. This choice was due to our goal to find molecules capable of correctly

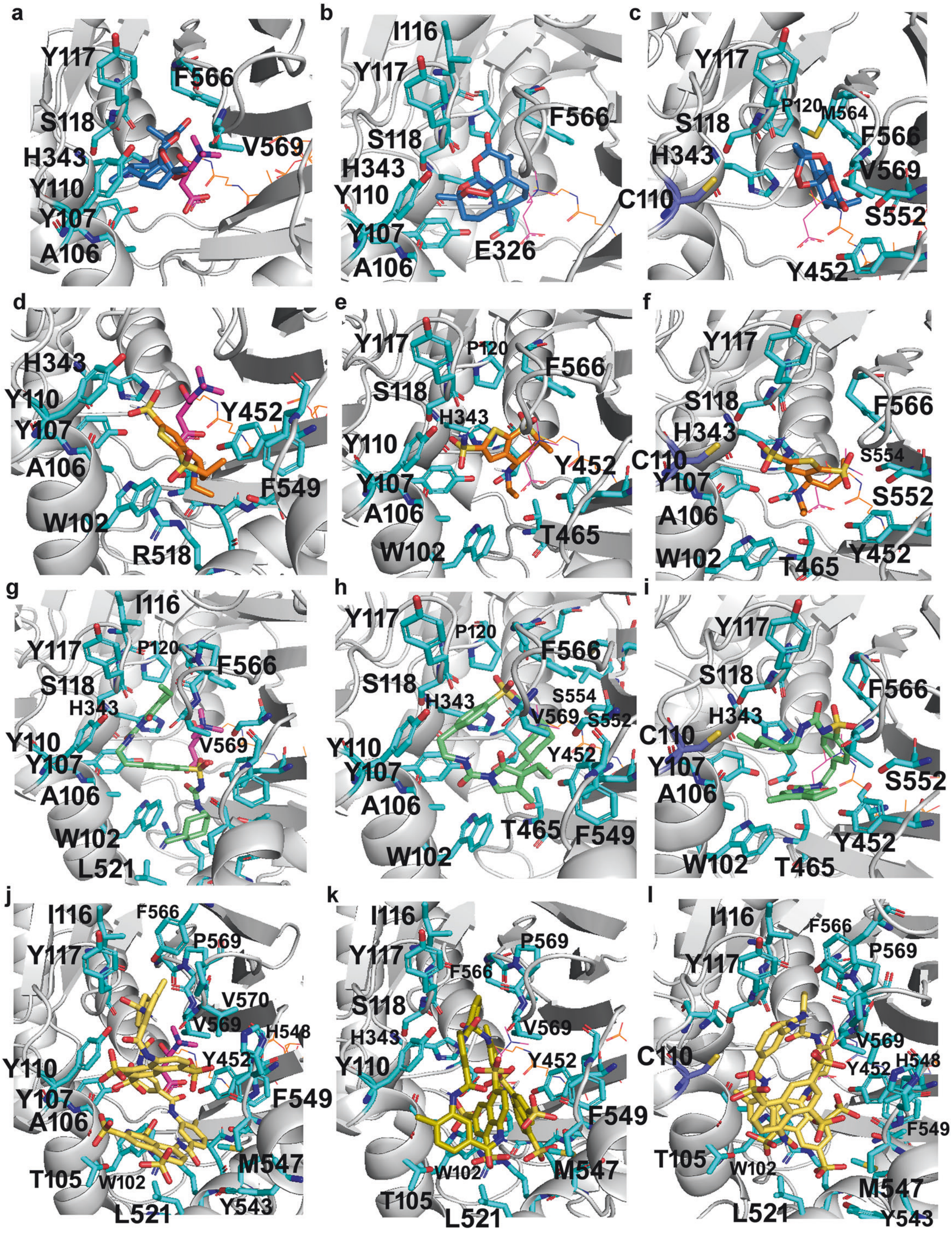

Fig. 4 Best poses of ligands artemisinin, dorzolamide, glimepiride, and suramin docked in the WT-CRAT in the presence of carnitine (left column), WT-CRAT in the absence of carnitine (middle column), and p.Tyr110Cys CRAT mutant in the absence of carnitine (right column). The best poses of artemisinin (**a**–**c**, blue sticks), dorzolamide (**d**–**f**, orange sticks), glimepiride (**g**–**i**, light green sticks), and suramin (**j**–**l**, light yellow sticks) docked in the WT-CRAT in the presence of carnitine, WT-CRAT in the absence of carnitine, and p.Tyr110Cys CRAT mutant in the absence of carnitine, respectively, are reported in the three panels of each row. Y110 is reported in cyan sticks, whereas C110 is reported in violet/yellow sticks. Carnitine from the crystallized structure is reported in magenta sticks in panels **a**, **d**, **g**, and **j**, whereas it is reported as a reference ligand in magenta lines in all the other panels, often behind the four docked molecules (as it could be observed by zooming-in the figure). CoA from the crystallized structure is reported in orange lines in all the panels. Residues within 4 Å from the carnitine reference ligand are reported in cyan sticks. The best poses of artemisinin, dorzolamide, and glimepiride were obtained by exploring the first described gridbox, whereas the reported best pose of suramin was obtained by exploring the second described larger gridbox.

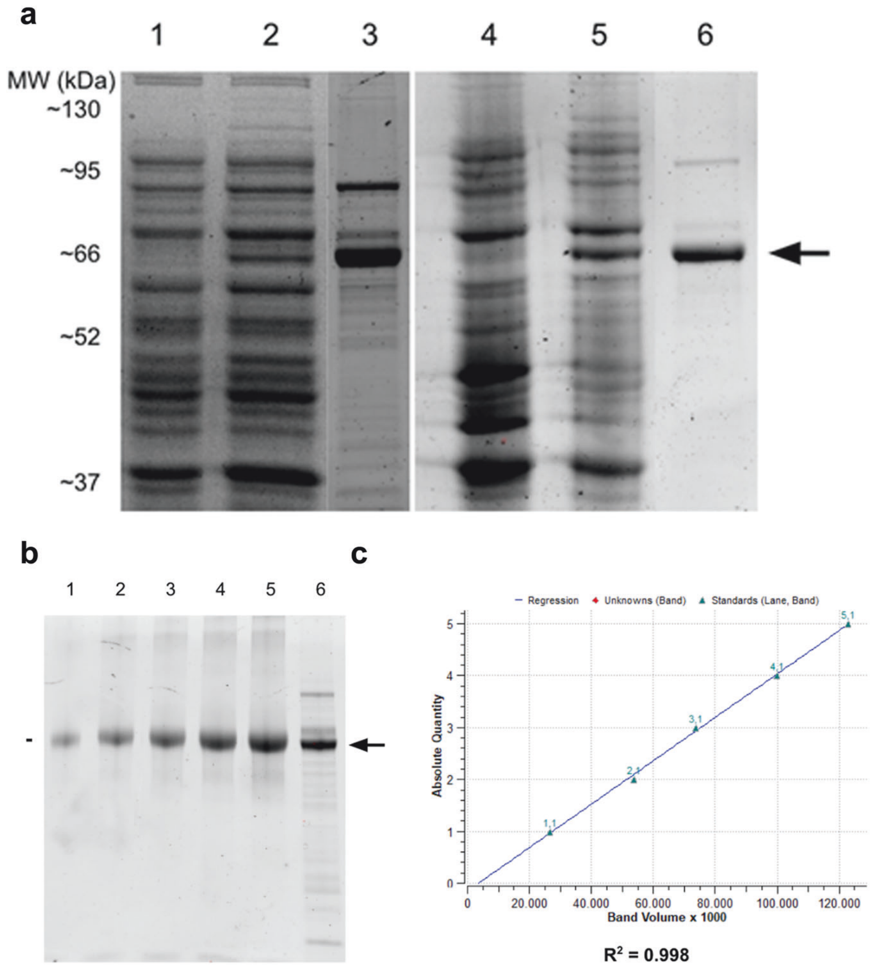

Fig. 5 **SDS-PAGE analysis of the recombinant CRAT proteins.** **a** Proteins were separated and stained with Coomassie Blue dye. Supernatant of the lysed bacteria expressing WT-CRAT before (1) and after IPTG induction (2); purified WT-CRAT (3); supernatant of the lysed bacteria expressing p.Tyr110Cys mutant before (4) and after IPTG induction (5); purified p.Tyr110Cys CRAT mutant (6). Black arrow indicates recombinant CRAT proteins. **b** SDS PAGE analysis for the quantification of WT-CRAT purified protein. 1, 2, 3, 4 and 5 μg of BSA (lane 1–5); purified WT-CRAT protein (lane 6). **c** Standard curve calculation through ImageLab software v6.1.

re-orienting the substrate within the pocket, even in the presence of the Y110C mutation.

Finally, the re-docking of the selected molecules on the WT-CRAT in the absence and presence of carnitine showed different binding poses of the investigated ligands, compared to those observed in the docking performed on the mutant proteins, however, artemisinin, most likely due to its rigidity, was the ligand that remained closer to Y110 or C110 in both docking series either in the presence or in the absence of the carnitine ligand, despite of what observed for dorzolamide (re-oriented towards the bottom of the investigated pocket in the presence of carnitine) and for the more hindering glimepiride (also re-oriented towards the bottom of the investigated pocket in the presence of carnitine).

This observation was important for our goal that was to find a molecule able to bind at the level of C110, for mimicking Y110 steric effect, to re-orient carnitine ligand towards its original position observed in the crystallized WT protein. In this regard, it is observed that artemisinin shows the lowest docking scores (in terms of LE_LC), compared to glimepiride and dorzolamide. Conversely, artemisinin shows the highest variation in the obtained docking scores in the presence and absence of carnitine, compared to glimepiride and dorzolamide. It is also observed that artemisinin cannot undergo torsions, at variance with dorzolamide and glimepiride. Conversely, artemisinin is the molecule that moves less in the explored pocket, either in the presence or in the absence of the carnitine substrate (as shown by residues in the 4 Å from the ligand highlighted after the docking simulations).

In vitro binding assays for validating docking predictions

Subsequent experimental validation (according to ref. [1]) of the four selected compounds (suramin, artemisinin, dorzolamide, and glimepiride), chosen among already approved drugs, confirmed the ability of two of them to modulate CRAT activity in vitro. These compounds exhibited dose-dependent effects on enzyme activity, supporting their specificity and potential therapeutic utility.

More in detail, the first bioactive compound, namely suramin, emerged as an inhibitor of CRAT activity either in the WT-CRAT or in the p.Tyr110Cys CRAT variant. In this regard, it can be speculated that low concentrations of suramin might be used for regulating the homeostasis of acetyl-CoA/acetyl-Carnitine pools (Fig. 8), particularly relevant in inflammatory diseases exhibiting mitochondrial dysfunction at the level of fatty acid translocation and metabolism [35–38]. However, it is important to note that suramin is able to target a lot of proteins, as observed for the inhibition of ADP/ATP carrier (and other carriers at a lower extent [10]), succinate dehydrogenase [39], or purine and peptide receptors [40]. Nevertheless, suramin's repurposing as a cancer therapeutic holds promise, if its effective concentration for

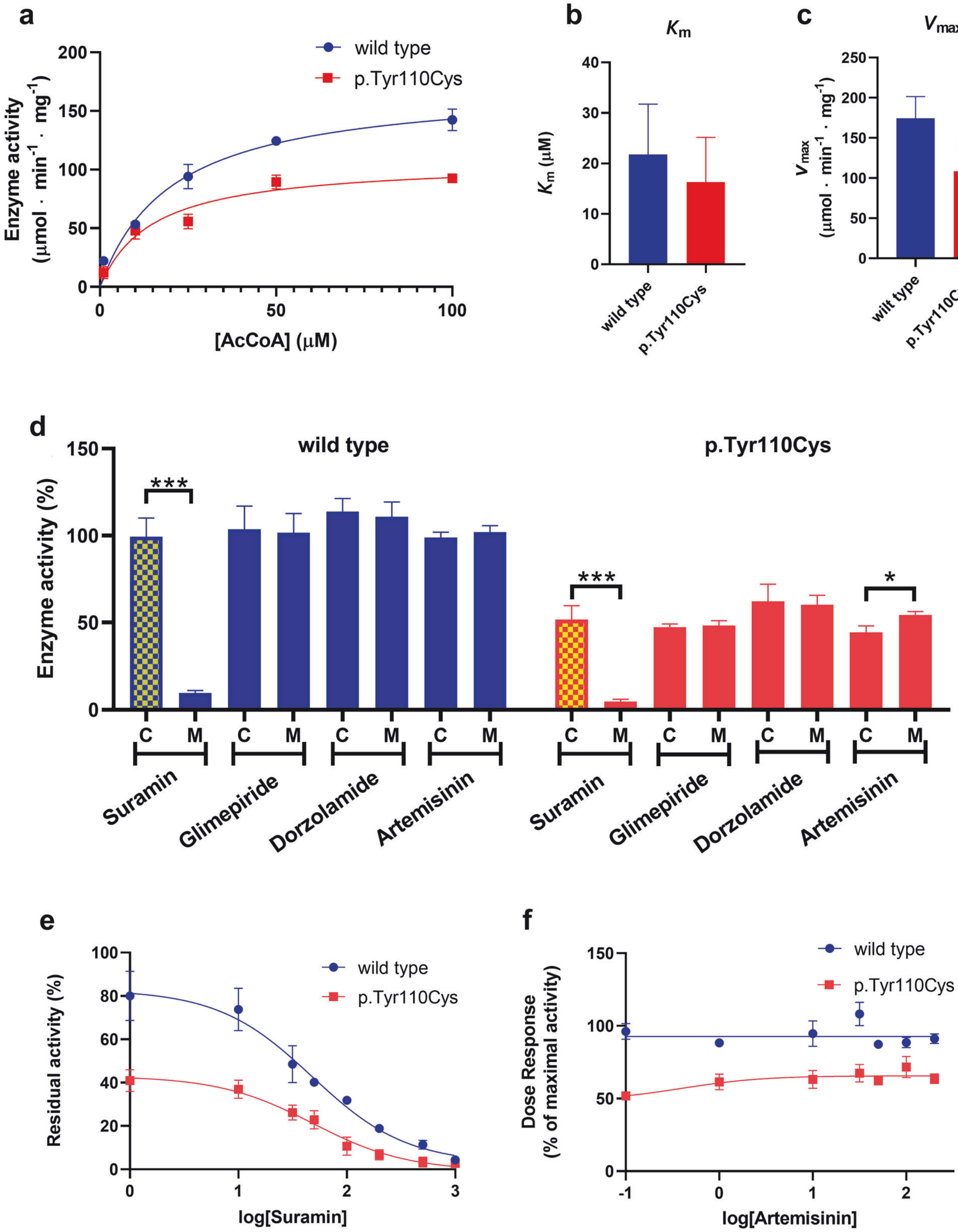

targeting CRAT can be achieved at lower doses than those historically used for treating other diseases, from neglected tropical diseases to cancer [41].

Artemisinin exhibited a weak activation of the recombinant CRAT mutant activity without significantly impacting WT-CRAT activity. Both suramin and artemisinin present opportunities for drug repurposing, with suramin potentially applicable in cancer therapy and artemisinin showing promise in treating CRAT-deficiency-related Leigh syndrome. Additionally, artemisinin's scaffold could serve as a scaffold for further modifications aimed at enhancing affinity towards the CRAT catalytic pocket.

Fig. 6 Estimation of the activity of WT-CRAT enzyme and p.Tyr110Cys CRAT variant in the presence and absence of selected molecules. Panel **a** Enzymatic activity of recombinant-purified WT-CRAT enzyme and p.Tyr110Cys CRAT variant proteins measured using the DTNB method, at different concentrations of acetyl-CoA (AcCoA). Michaelis–Menten (MM) constant K_m (**b**) and maximum activity rate V_{max} (**c**) of recombinant-purified WT-CRAT and p.Tyr110Cys CRAT proteins. MM parameter estimations were conducted in GraphPad Prism. Data are presented as mean ± SEM of at least three independent experiments. "***" indicates nonoverlapping 95% confidence intervals between the V_{max} determined for the WT-CRAT protein and for the p.Tyr110Cys variant. Panel **d** The activity (%) of WT-CRAT and p.Tyr110Cys measured in the absence (C, control) or presence (M, molecule) of each tested molecule. Data are presented as mean ± SEM of three independent experiments. Statistical analysis was performed using *t*-test between corresponding control vs. molecule results. $^{*}P < 0.05$; $^{***}P < 0.001$. Concentration-dependent inhibition (**e**) or stimulation (**f**) of WT-CRAT (blue circles) or p.Tyr110Cys CRAT (red squares) activity mediated by suramin (**e**) or artemisinin (**f**) expressed as percentage of the WT-CRAT activity in the absence of molecules set at 100% (the activity of p.Tyr110Cys CRAT mutant in the absence of molecules was 45% of the WT-CRAT, estimated for comparative purposes). Experiments were conducted in K_m conditions as determined in panel **a**. The reaction was started by adding 2 mM carnitine. Suramin was tested at the concentrations 1, 10, 30, 50, 100, 200, 500 and 1000 μM. Artemisinin was tested at the concentrations 0.1, 1, 10, 30, 50, 100 and 200 μM. Notably, the percentage of DMSO in the tests with artemisinin was 0.2% (final concentration in cuvette) for all the tested concentrations of the artemisinin. Values are presented as means ± SEM derived from three independent experiments.

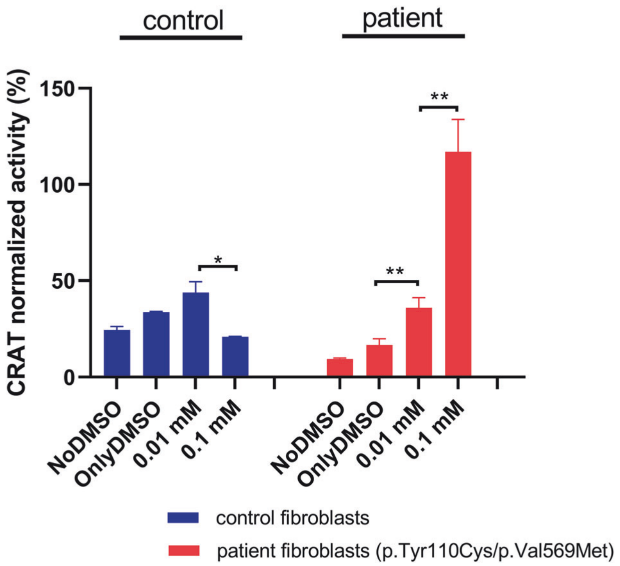

Fig. 7 Artemisinin concentration-dependent stimulation of CRAT activity. The estimated CRAT activity is normalized to CS activity in control fibroblasts and patient fibroblasts (carrying the compound heterozygous missense variants p.Tyr110Cys and p.Val569Met in the CRAT gene). Controls in DMSO were produced since artemisin was solubilized in DMSO. The final concentration of DMSO in the assay was 1%. Values are presented as means ± SEM derived from at least three independent experiments. Statistical analysis was performed using *t*- test. $^{*}P < 0.05$; $^{**}P < 0.01$.

The above reported in silico/in vitro observations, let us speculate that the rigid artemisinin is better in re-orienting carnitine ligand in the mutated protein towards its original position. In addition, artemisinin rigidity makes artemisinin exit from carnitine binding pocket more difficult also in the presence of carnitine, at variance with the larger glimepiride and dorzolamide showing a larger number of torsions, that allow glimepiride and dorzolamide exiting carnitine binding pocket in the presence of the carnitine substrate, despite of the calculated higher docking-scores.

Additionally, assays conducted on cell lysates provided evidence of the artemisinin ability to influence CRAT activity in a cellular context, highlighting its potential for therapeutic intervention in mitochondrial disorders. Indeed, our experimental validation of compound activity in patient cell lysates revealed a partially CRAT restored function, also in the context of patient cells carrying the compound heterozygous p.Tyr110Cys and p.Val569Met missense variants in the CRAT gene [1]. This observation underscores the clinical relevance of our findings and suggests the therapeutic potential of an early genetic diagnosis associated to virtual screening of drug libraries aiming to restore the function of impaired proteins responsible for severe pathological conditions.

Pharmacokinetic and pharmacodynamic considerations for the clinical use of suramin and artemisinin

While our virtual screening has identified suramin and artemisinin as promising candidates for repurposing in CRAT deficiency and oxidative-dependent cancers, it is crucial to consider their pharmacokinetic and pharmacodynamic profiles, as these factors directly impact their clinical applicability. Suramin, despite its efficacy in inhibiting oxidative-dependent pathways, exhibits poor oral bioavailability and is administered intravenously to achieve therapeutic plasma concentrations [42]. Its long half-life (~50 days) is attributed to its limited metabolism, as the drug is primarily excreted unchanged via the kidneys. However, this prolonged exposure increases the risk of dose-dependent toxicity, with side effects ranging from nausea and fatigue to more severe complications such as renal toxicity and peripheral neuropathy, particularly at higher doses used in cancer therapies [42, 43]. Conversely, it has also been reported that suramin can inhibit renal fibrosis in chronic kidney disease [44].

On the other hand, artemisinin, while promising for treating CRAT deficiency due to its oxidative stress-modulating properties, faces challenges with poor oral bioavailability owing to rapid first-pass metabolism in the liver [45]. Although semi-synthetic derivatives like artemether enhance its absorption, artemisinin's short half-life (1–3 h) necessitates frequent dosing. Its rapid metabolism to dihydroartemisinin, the active form, also limits sustained therapeutic exposure [46]. While generally well-tolerated, prolonged or high-dose use of artemisinin have been linked to rare instances of neurotoxicity [47] and hepatotoxicity [48, 49]. Therefore, both drugs, while clinically viable, present challenges in bioavailability, metabolic stability, and potential toxicity, which must be carefully considered when designing future therapeutic protocols.

Conclusive remarks

The reported study underscores the utility of molecular modeling tools in elucidating protein structure-function relationships, as well as protein-ligand [10, 50, 51] or protein-protein [52, 53] interactions in guiding drug discovery efforts. It should also be noticed that longer molecular dynamics simulations can provide new insights about transient binding pockets to be exploited by potential modulators. MD based approaches can also provide data about the stability of the interactions between the investigated WT and mutant proteins and the predicted high affinity ligands.

Remarkably, in the context of drug repurposing within compassionate use programs, approved drugs that show high binding affinity for new targets through in silico studies can be used to treat patients with diseases lacking established therapies,

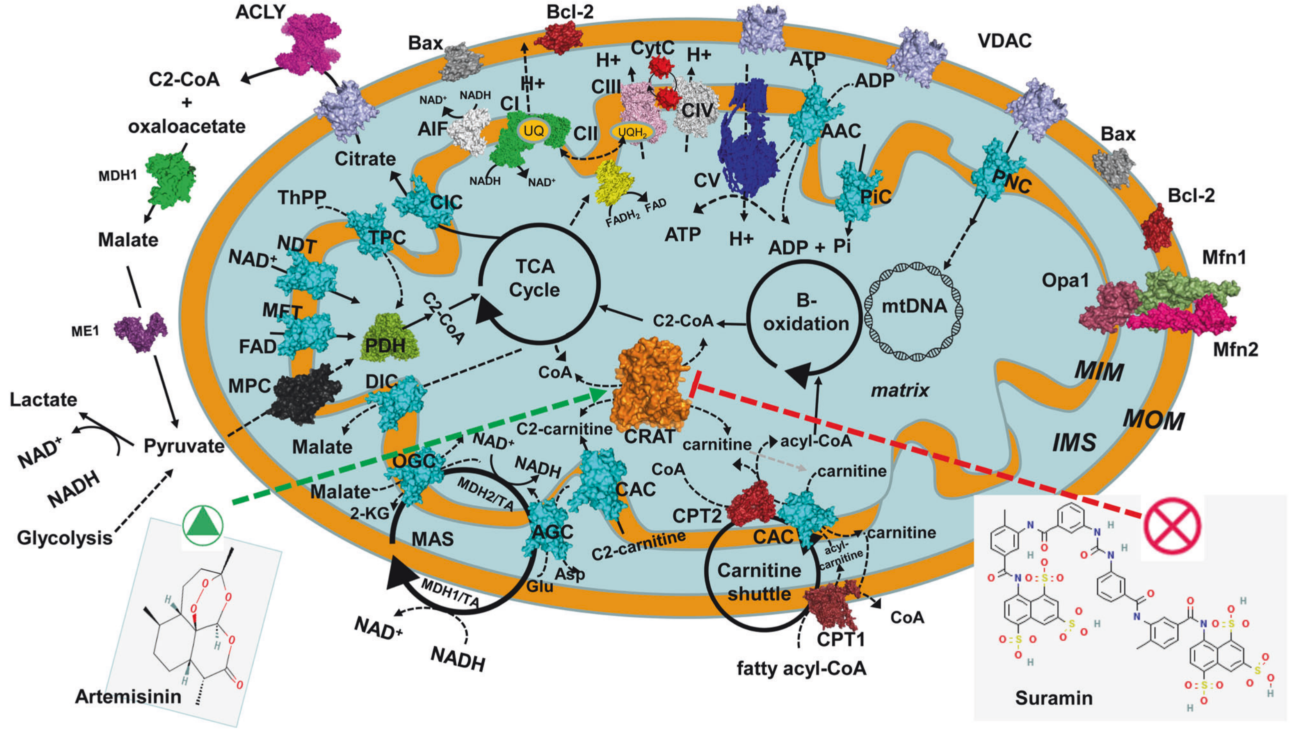

Fig. 8 Scheme of a mitochondrion with a set of representative proteins, pathways and cycles. CRAT, protein of the carnitine shuttle, respiratory chain complexes, mitochondrial transporters and other proteins are reported in surface representation and labeled. CRAT (based on the human crystallized structure 1nm8.pdb) is reported in orange surface representation; CPT1 and CPT2 (both based on the *R. norvegicus* crystallized structure 4ep9.pdb) in dark violet; ATP synthase (CV) is reported in blue (based on the Bos taurus crystallized structure 6zqn.pdb). Mitochondrial carriers are reported in cyan (based on the 3D structure of the bovine ADP/ATP carrier, 1okc.pdb). VDAC is reported in pink (based on the 3D structure of the human 2jk4.pdb). Bax (based on the 3D structure of the human 4s0o.pdb) and Bak/Bcl-2 (based on the human crystallized structure 2yv6.pdb) are reported in dark gray and firebrick, respectively. MPC (an in-house developed 3D comparative model, data not published) is reported in black; PDH in light green (based on the human crystallized structure 6cfo.pdb); AIF in white (based on the human crystallized structure 4bur.pdb). Complex I (CI, based on the Ovis aries crystallized structure 5lnk.pdb), complex II (CII, based on the Sus scrofa scrofa 3aef.pdb), complex III (CIII, based on the O. aries 6q9e.pdb), complex IV (CIV) (together with CytC in red, based on the bovine crystallized structure 5iy5.pdb) are reported in green, yellow, magenta and gray, respectively, Opa1 (based on the human crystallized structure 6jtg.pdb) is reported in dark magenta; Mfn1 (based on the human crystallized structure 5gns.pdb) in dark green; Mfn2 (based on the human crystallized structure 6jfk.pdb) in hot-pink, according to PyMOL colors. Black circular arrows indicate cyclic pathways. Red arrows indicate impaired pathways or reactions. Black solid/dashed lines indicate the possible direction of the reported reactions. C2-CoA acetyl-CoA, C2-carnitine acetyl-carnitine, MIM mitochondrial inner membrane, MOM mitochondrial outer membrane, IMS intermembrane space, UQ ubiquinone, AAC ADP/ATP carrier, coded in H. sapiens by SLC25A4, SLC25A5, SLC25A6, SLC25A31, TPC thiamine pyrophosphate carrier, coded by SLC25A19, CAC carnitine/acyl-carnitine carrier, coded by SLC25A20, ORC ornithine carrier, coded by SLC25A15 (or SLC25A2), AGC aspartate/glutamate carrier, coded by SLC25A12 and SLC25A13, DIC dicarboxylate carrier, coded by SLC25A10, NDT assumed to be the NAD$^+$ carrier, coded by SLC25A51, MFT assumed to be the FAD (folate/riboflavin) carrier, coded by SLC25A32, OGC malate/2-oxoglutarate carrier, coded by SLC25A11, CIC citrate carrier, coded by SLC25A1, PiC phosphate carrier, coded by SLC25A3, MAS malate/aspartate shuttle, TCA tricarboxylic acid cycle, Bax Bcl-2 associated X protein, Bak Bcl-2 antagonist/killer-1, Bcl-2 B-cell lymphoma-2, MDH1 cytosolic malate dehydrogenase 1, ME1 malic enzyme 1, MPC mitochondrial pyruvate carrier, PDH pyruvate dehydrogenase, CypD cyclophilin D, CytC cytochrome *c*, VDAC voltage-dependent anion channel, AIF apoptosis-inducing factor, PNC pyrimidine nucleotide carrier, coded in H. sapiens by SLC25A33 and SLC25A36. The green arrow for artemisinin and the red arrow for suramin, indicate the ability of artemisinin to stimulate the activity of p.Tyr110Cys variant and the ability of suramin to inhibit both the WT-CRAT and the p.Tyr110Cys variant.

as it was for the recent COVID-19 pandemics [53, 54]. However, it is crucial to validate these computational findings by experimentally testing the affinity of the ligands for the hypothesized targeted recombinant proteins, particularly in cases beyond compassionate use [9, 55].

More in general, our findings highlight a strategy for dealing with pathological missense variants causing a partial loss of function, through the modulation of protein activity by targeting protein binding regions affected by specific mutations.

The protocol described in this manuscript for targeting the CRAT region hosting the pathological mutation, might also be employed for targeting the impaired regions of other enzymes, transporters, and protein complexes associated to the onset of Leigh syndrome or other neuromuscular degenerative diseases, including severe mitochondrial diseases [2, 6, 12, 56–59], aiming to restore the impaired metabolic pathway for rescuing mitochondrial function for slowing-down the neuromuscular degeneration associated with these devastating diseases.

By bridging computational and experimental approaches, our study offers insights into personalized therapeutic strategies aimed at restoring mitochondrial function and improving clinical outcomes in patients affected by mitochondrial disorders. Moreover, our approach represents a potential application of the concept of "theragnosis", already applied in other biomedical research fields [60], wherein therapeutic interventions can be guided by diagnostic information, also for mitochondrial diseases, thereby enabling personalized treatment strategies tailored to individual patient profiles [2, 12]. This concept of theragnosis represents a paradigm shift in precision medicine, offering new avenues for the development of targeted therapies and the optimization of patient care in the era of molecular medicine [2].

ACKNOWLEDGEMENTS

This research was supported by EU funding within the MUR PNRR Extended Partnership initiative on Emerging Infectious Diseases (Project No. PE00000007, INF-ACT) and MUR PNRR National Center for Gene Therapy and Drugs based on RNA Technology (Project No. CN_00000041). The authors would also like to thank for the IT resources made available by ReCaS (https://www.recas-bari.it/index.php/en/), a project funded by the MIUR (Italian Ministry for Education, University and Research) in the "PON Ricerca e Competitivita 2007–2013-Azione I-Interventi di rafforzamento strutturale" PONa3_00052, Avviso 254/Ric, University of Bari. In addition, the authors would like to thank the Italian Association for Mitochondrial Research – AIRM (https://www.mitoairm.it/) and the Italian Association of patients affected by Mitochondrial Diseases MITOCON (https://www.mitocon.it/). This manuscript is dedicated to Elena, Maya, Irene and all the other mitopatients.

AUTHOR CONTRIBUTIONS

CLP, ADG, MV did the conceptualization; LCB, MNS, LL, VS, ST, SB, ALF, DIDL, MM contributed to the data curation and formal analysis; LG, VP, MV, CLP, ADG did the supervision. LCB, MV, ADG, and CLP wrote the original draft; all the authors contributed in writing-reviewing and editing the text.

ADDITIONAL INFORMATION

Competing interests: The authors declare no competing interests.

REFERENCES

1. Laera L, Punzi G, Porcelli V, Gambacorta N, Trisolini L, Pierri CL, et al. CRAT missense variants cause abnormal carnitine acetyltransferase function in an early-onset case of Leigh syndrome. Hum Mutat. 2020;41:110–4.
2. Tragni V, Primiano G, Tummolo A, Cafferati Beltrame L, La Piana G, Sgobba MN, et al. Personalized medicine in mitochondrial health and disease: molecular basis of therapeutic approaches based on nutritional supplements and their analogs. Molecules. 2022;27:3494.
3. Lake NJ, Compton AG, Rahman S, Thorburn DR. Leigh syndrome: One disorder, more than 75 monogenic causes. Ann Neurol. 2016. https://doi.org/10.1002/ana.24551
4. Di Mauro S. Mitochondrial encephalomyopathies: Where next? Acta Myologica. 2000;19:181–8.
5. Hirano M. Leigh Syndrome. In: Encyclopedia of Movement Disorders. 2010. https://doi.org/10.1016/B978-0-12-374105-9.00339-7
6. Punzi G, Porcelli V, Ruggiu M, Hossain MF, Menga A, Scarcia P, et al. SLC25A10 biallelic mutations in intractable epileptic encephalopathy with complex I deficiency. Hum Mol Genet. 2018;27:499–504.
7. Muoio DM, Noland RC, Kovalik JP, Seiler SE, Davies MN, DeBalsi KL, et al. Muscle-specific deletion of carnitine acetyltransferase compromises glucose tolerance and metabolic flexibility. Cell Metab. 2012;15:764–77. https://doi.org/10.1016/j.cmet.2012.04.005
8. Reichenbach A, Stark R, Mequinion M, Denis R, Goularte JF, Clarke RE, et al. AgRP neurons require carnitine acetyltransferase to regulate metabolic flexibility and peripheral nutrient partitioning. Cell Rep. 2018;22:1745–59. https://doi.org/10.1016/j.celrep.2018.01.067
9. Pierri CL, Parisi G, Porcelli V. Computational approaches for protein function prediction: A combined strategy from multiple sequence alignment to molecular docking-based virtual screening. Biochim Biophys Acta Proteins Proteom. 2010;1804:1695–712.
10. Todisco S, Di Noia MA, Onofrio A, Parisi G, Punzi G, Redavid G, et al. Identification of new highly selective inhibitors of the human ADP/ATP carriers by molecular docking and in vitro transport assays. Biochem Pharmacol. 2016;100:112–32.
11. Trisolini L, Gambacorta N, Gorgoglione R, Montaruli M, Laera L, Colella F, et al. FAD/NADH dependent oxidoreductases: from different amino acid sequences to similar protein shapes for playing an ancient function. J Clin Med. 2019;8:2117.
12. Todisco S, Musio B, Pesce V, Cavalluzzi MM, Petrosillo G, La Piana G, et al. Targeting mitochondrial impairment for the treatment of cardiovascular diseases: From hypertension to ischemia-reperfusion injury, searching for new pharmacological targets. Biochem Pharmacol. 2023;208:115405. https://doi.org/10.1016/j.bcp.2022.115405
13. Tragni V, Cotugno P, De Grassi A, Cavalluzzi MM, Mincuzzi A, Lentini G, et al. Targeting *Penicillium expansum* GMC oxidoreductase with high affinity small molecules for reducing patulin production. Biology. 2020;10:21.
14. Srere PA. [1] Citrate synthase. [EC 4.1.3.7. Citrate oxaloacetate-lyase (CoA-acetylating)]. Methods Enzymol. 1969;3–11. https://doi.org/10.1016/0076-6879(69)13005-0
15. Suparmi S, de Haan L, Spenkelink A, Louisse J, Beekmann K, Rietjens I. Combining in vitro data and physiologically based kinetic modeling facilitates reverse dosimetry to define in vivo dose–response curves for Bixin- and crocetin-induced activation of PPARγ in humans. Mol Nutr Food Res. 2020;64:1900880. https://doi.org/10.1002/mnfr.201900880
16. Wu D, Govindasamy L, Lian W, Gu Y, Kukar T, Agbandje-McKenna M, et al. Structure of human carnitine acetyltransferase: molecular basis for fatty acyl transfer. J Biol Chem. 2003;278:13159–65. https://doi.org/10.1074/jbc.M212356200
17. Hsiao YS, Jogl G, Tong L. Crystal structures of murine carnitine acetyltransferase in ternary complexes with its substrates. J Biol Chem. 2006;281:28480–7. https://doi.org/10.1074/jbc.M602622200
18. Cosconati S, Forli S, Perryman AL, Harris R, Goodsell DS, Olson AJ. Virtual screening with AutoDock: theory and practice. Expert Opin Drug Discov. 2010;5:597–607.
19. Forli S, Huey R, Pique ME, Sanner MF, Goodsell DS, Olson AJ. Computational protein-ligand docking and virtual drug screening with the AutoDock suite. Nat Protoc. 2016;11:905–19. https://doi.org/10.1038/nprot.2016.051
20. Ertl P, Jelfs S. Designing drugs on the internet? Free web tools and services supporting medicinal chemistry. Curr Top Med Chem. 2007;7:1491–501. https://doi.org/10.2174/156802607782194707
21. O'boyle NM, Banck M, James CA, Morley C, Vandermeersch T, Hutchison GR. Open Babel: An Open chemical toolbox. J Cheminformatics. 2011;3:33. https://doi.org/10.1186/1758-2946-3-33
22. Llopis J, McCaffery JM, Miyawaki A, Farquhar MG, Tsien RY. Measurement of cytosolic, mitochondrial, and Golgi pH in single living cells with green fluorescent proteins. Proc Natl Acad Sci USA. 1998;95:6803–8. https://doi.org/10.1073/pnas.95.12.6803
23. Matsuyama S, Llopis J, Deveraux QL, Tsien RY, Reed JC. Changes in intramitochondrial and cytosolic pH: Early events that modulate caspase activation during apoptosis. Nat Cell Biol. 2000;2:318–25. https://doi.org/10.1038/35014006
24. Cano Abad MF, Di Benedetto G, Magalhães PJ, Filippin L, Pozzan T. Mitochondrial pH monitored by a new engineered green fluorescent protein mutant. J Biol Chem. 2004;279:11521–9. https://doi.org/10.1074/jbc.M306766200
25. Morris GM, Huey R, Olson AJ. Using AutoDock for ligand-receptor docking. Curr Protoc Bioinforma. 2008;Chapter 8:Unit 8.14.
26. Morris GM, Goodsell DS, Halliday RS, Huey R, Hart WE, Belew RK, et al. Automated docking using a Lamarckian genetic algorithm and an empirical binding free energy function. J Comput Chem. 1998;19:1639–62.
27. Mendez D, Gaulton A, Bento AP, Chambers J, De Veij M, Félix E, et al. ChEMBL: Towards direct deposition of bioassay data. Nucleic Acids Res. 2019;47:930. https://doi.org/10.1093/nar/gky1075
28. De Grassi A, Lanave C, Saccone C. Evolution of ATP synthase subunit c and cytochrome c gene families in selected Metazoan classes. Gene. 2006;371:224–33. https://doi.org/10.1016/j.gene.2005.11.022
29. Saccone C, Lanave C, De Grassi A. Metazoan OXPHOS gene families: evolutionary forces at the level of mitochondrial and nuclear genomes. Biochim Biophys Acta. 2006;1757:1171–8.
30. Roger AJ, Muñoz-Gómez SA, Kamikawa R. The origin and diversification of mitochondria. Curr Biol. 2017;27:1177. https://doi.org/10.1016/j.cub.2017.09.015
31. Schubert MB, Vilarinho L. Molecular basis of Leigh syndrome: a current look. Orphanet J Rare Dis. 2020;15:31.
32. Finsterer J. Leigh and Leigh-like syndrome in children and adults. Pediatric Neurol. 2008. https://doi.org/10.1016/j.pediatrneurol.2008.07.013
33. Pierri CL, De Grassi A, Turi A. Lattices for ab initio protein structure prediction. Proteins. 2008;73:351–61.
34. Chen H, Gu F, Huang Z. Improved Chou-Fasman method for protein secondary structure prediction. BMC Bioinforma. 2006;7:S14.
35. Ghilardi G, Paruzzo L, Svoboda J, Chong EA, Shestov AA, Chen L, et al. Bendamustine lymphodepletion before axicabtagene ciloleucel is safe and associates with reduced inflammatory cytokines. Blood Adv. 2024;8:653–66. https://doi.org/10.1182/bloodadvances.2023011492
36. Giangregorio N, Pierri CL, Tonazzi A, Incampo G, Tragni V, De Grassi A, et al. Proline/Glycine residues of the PG-levels guide conformational changes along the transport cycle in the mitochondrial carnitine/acylcarnitine carrier (SLC25A20). Int J Biol Macromol. 2022;221:1453–65.
37. Santarsiero A, Convertini P, Todisco S, Pierri CL, De Grassi A, Williams NC, et al. ACLY nuclear translocation in human macrophages drives proinflammatory gene expression by NF-κB acetylation. Cells. 2021;10. https://doi.org/10.3390/cells10112962
38. Infantino V, Pierri CL, Iacobazzi V. Metabolic routes in inflammation: the citrate pathway and its potential as therapeutic target. Curr Med Chem. 2018;26:7104–16. https://doi.org/10.2174/0929867325666180510124558
39. Roveri OA, Franke de Cazzulo BM, Cazzulo JJ. Inhibition by suramin of oxidative phosphorylation in *Crithidia fasciculata*. Comp Biochem Physiol Part B Biochem. 1982;71:611–6. https://doi.org/10.1016/0305-0491(82)90470-9

40. Jenkinson KM, Reid JJ. The P2-purinoceptor antagonist suramin is a competitive antagonist at vasoactive intestinal peptide receptors in the rat gastric fundus. Br J Pharmacol. 2000;130:1632–8. https://doi.org/10.1038/sj.bjp.0703482
41. Wiedemar N, Hauser DA, Mäser P. 100 years of suramin. Antimicrob Agents Chemother.2020;64: e0116819. https://doi.org/10.1128/AAC.01168-19
42. Ogden A, Wientjes MG, Au JLS. Suramin as a chemosensitizer: oral pharmacokinetics in rats. Pharmacol Res. 2004;21:2058–63. https://doi.org/10.1023/B:PHAM.0000048197.77546.75
43. Wu G, Zhou H, Lv D, Zheng R, Wu L, Yu S, et al. Phase I, single-dose study to assess the pharmacokinetics and safety of suramin in healthy Chinese volunteers. Drug Des Devel Ther. 2023;17:2051–61. https://doi.org/10.2147/DDDT.S416325
44. Liu N, Tolbert E, Pang M, Ponnusamy M, Yan H, Zhuang S. Suramin inhibits renal fibrosis in chronic kidney disease. J Am Soc Nephrol. 2011;22:1064–75. https://doi.org/10.1681/ASN.2010090956
45. Fu C, Shi H, Chen H, Zhang K, Wang M, Qiu F. Oral bioavailability comparison of artemisinin, deoxyartemisinin, and 10-deoxoartemisinin based on computer simulations and pharmacokinetics in rats. ACS Omega. 2021;6:889–99. https://doi.org/10.1021/acsomega.0c05465
46. Eastman RT, Fidock DA. Artemisinin-based combination therapies: A vital tool in efforts to eliminate malaria. Nat Rev Microbiol. 2009;7:864–74. https://doi.org/10.1038/nrmicro2239
47. Toovey S. Are currently deployed artemisinins neurotoxic? Toxicol Lett. 2006;166:95–104. https://doi.org/10.1016/j.toxlet.2006.06.001
48. Schramm B, Valeh P, Baudin E, Mazinda CS, Smith R, Pinoges L, et al. Tolerability and safety of artesunate-amodiaquine and artemether- lumefantrine fixed dose combinations for the treatment of uncomplicated *Plasmodium falciparum* malaria: two open-label, randomized trials in Nimba County, Liberia. Malar J. 2013;12:250. https://doi.org/10.1186/1475-2875-12-250
49. Gordi T, Lepist EI. Artemisinin derivatives: Toxic for laboratory animals, safe for humans? Toxicol Lett. 2004;147:99–107. https://doi.org/10.1016/j.toxlet.2003.12.009
50. Porcelli L, Di Fonte R, Pierri CL, Fucci L, Saponaro C, Armenio A, et al. BRAF-V600E;K601Q metastatic melanoma patient-derived organoids and docking analysis to predict the response to targeted therapy. Pharmacol Res. 2022;182:106323. https://doi.org/10.1016/j.phrs.2022.106323
51. Menga A, Serra M, Todisco S, Riera-Domingo C, Ammarah U, Ehling M, et al. Glufosinate constrains synchronous and metachronous metastasis by promoting anti-tumor macrophages. EMBO Mol Med. 2020;12:11210. https://doi.org/10.15252/emmm.201911210
52. Pierri CL, Bossis F, Punzi G, De Grassi A, Cetrone M, Parisi G, et al. Molecular modeling of antibodies for the treatment of TNFα-related immunological diseases. Pharmacol Res Perspect. 2016;4:e00197.
53. Tragni V, Preziusi F, Laera L, Onofrio A, Mercurio I, Todisco S, et al. Modeling SARS-CoV-2 spike/ACE2 protein–protein interactions for predicting the binding affinity of new spike variants for ACE2, and novel ACE2 structurally related human protein targets, for COVID-19 handling in the 3PM context. EPMA J. 2022;13:149–75. https://doi.org/10.1007/s13167-021-00267-w
54. Jonker AH, O'Connor D, Cavaller-Bellaubi M, Fetro C, Gogou M, 't Hoen P, et al. Drug repurposing for rare: progress and opportunities for the rare disease community. Front Med. 2024;11:1352803. https://doi.org/10.3389/fmed.2024.1352803
55. Jin G, Wong STC. Toward better drug repositioning: prioritizing and integrating existing methods into efficient pipelines. Drug Discov Today. 2014;19:637-44. https://doi.org/10.1016/j.drudis.2013.11.005
56. Shteyer E, Edvardson S, Wynia-Smith SL, Pierri CL, Zangen T, Hashavya S, et al. Truncating mutation in the nitric oxide synthase 1 gene is associated with infantile achalasia. Gastroenterology. 2015;148:533–6.e4.
57. Pop A, Williams M, Struys EA, Monné M, Jansen E, De Grassi A, et al. An overview of combined D-2- and L-2-hydroxyglutaric aciduria: functional analysis of CIC variants. J Inherit Metab Dis. 2018;41:169–80.
58. Carrozzo R, Torraco A, Fiermonte G, Martinelli D, Di Nottia M, Rizza T, et al. Riboflavin responsive mitochondrial myopathy is a new phenotype of dihydrolipoamide dehydrogenase deficiency. The chaperon-like effect of vitamin B2. Mitochondrion. 2014;18:49–57.
59. Fichtman B, Harel T, Biran N, Zagairy F, Applegate CD, Salzberg Y, et al. Pathogenic variants in NUP214 cause “plugged” nuclear pore channels and acute febrile encephalopathy. Am J Hum Genet. 2019;105:48–64.
60. Perrone MG, Luisi O, De Grassi A, Ferorelli S, Cormio G, Scilimati A. Translational theragnosis of ovarian cancer: where do we stand? Curr Med Chem. 2019;27:5675–715. https://doi.org/10.2174/0929867326666190816232330